Ocean Feedback in Response to 6 kyr BP Insolation

P. Braconnot, O. Marti, S. Joussaume, Y. Leclainche

Ocean Feedback in Response to 6 kyr BP Insolation*

P. BRACONNOT, O. MARTI, S. JOUSSAUME, AND Y. LECLAINCHE

Laboratoire des Sciences du Climat et de l'Environnement, Unité Mixte de Recherche CEA-CNRS, Orme des Merisiers, Gif-sur-Yvette, France

(Manuscript received 4 January 1999, in final form 14 July 1999)

ABSTRACT

The role of the ocean in the 6 kyr BP climate change is investigated by comparing a coupled ocean–atmosphere simulation and a simulation with the same atmospheric component for which SSTs are kept to the modern ones. For these simulations, Earth's orbital parameters have been changed from their current values to those valid 6 kyr ago. The resulting change in insolation strengthens the seasonal cycle in the Northern Hemisphere, and the summer African and Asian monsoons are more vigorous.

The results show that the summer monsoon flow penetrates farther north into the Sahara when ocean feedbacks are included. The SST response lags by 2–3 months the insolation forcing. This delay has an impact on the timing of the monsoon change. In most coastal regions, the climate response is very different, and even of opposite sign, between the coupled and atmosphere-alone experiments, stressing the climatic impact of the ocean in these regions.

The impact of the interactive ocean on the poleward heat transport is also analyzed. The 6 kyr BP insolation change creates seasonal perturbations of the zonal mean solar forcing, which in turn affects the meridional heat transport. The change in the ocean heat transport is as large as that of the atmosphere in most latitudes and seasons. The largest variations in the ocean occur in the Tropics and are dominated by changes in the Ekman transport. The coupled and atmosphere-alone simulations exhibit different changes in atmosphere heat transport, although they have almost the same change in net heat flux at the top of the atmosphere.

1. Introduction

Monsoon is part of the atmospheric heat engine and contributes to the redistribution of heat from the equator to the poles. It is very responsive to changes in insolation induced by variations of Earth's orbital elements that alter the land–sea temperature contrast (Kutzbach and Otto-Bliesner 1982; Kutzbach and Guetter 1986; Royer et al. 1984; Prell and Kutzbach 1987; Dong et al. 1996; de Noblet et al. 1996). Using a simple energy balance–mixed layer model, Lindzen and Pan (1994) have noted that the precession of the equinoxes can lead to profound variations in the transport of heat from the Tropics to higher latitudes, because the intensity of the Hadley circulation depends strongly on the maximum displacement of the zonally averaged surface temperature (Hou 1993). Rind (1998) has also shown that the latitudinal temperature gradient governs the Hadley cell intensity, whereas the mean temperature governs the Hadley extent.

Differences in Earth's orbital parameters, and mainly the precession of the equinoxes, between 6 kyr BP and present day cause an amplification of the seasonal cycle in the Northern Hemisphere and strengthen the summer monsoon activity (Kutzbach et al. 1993; Hall and Valdes 1997; Hewitt and Mitchell 1996), thereby enhancing heat transfer from the Northern Hemisphere (NH) to the Southern Hemisphere (SH; Masson and Joussaume 1997). Marine records suggest that for this period departures from modern sea surface temperature (SST) are small and within the error bars of temperature reconstructions, except at high northern latitudes and in a few coastal regions (e.g., Ruddiman and Mix 1993). As a first approximation, it was thus appropriate to keep SSTs as they are today to study the climatic response to the 6 kyr BP insolation with atmospheric general circulation models. The 6 kyr BP simulations of the Paleoclimate Modeling Intercomparison Project (PMIP) have been performed with this assumption (Joussaume and Taylor 1995). They all exhibit a more vigorous monsoon, which is consistent with the wettening recorded by paleoclimate data over land in now-arid regions extending from North Africa to Southeast Asia (Wright et al. 1993; Jolly et al. 1998; Yu and Harrison 1996). However, PMIP simulations underestimate the northward penetration of

* Laboratoire des Sciences du Climat et de l'Environnement Contribution Number 0289A.

Corresponding author address: P. Braconnot, LSCE, Unité Mixte de Recherche CEA-CNRS, Orme des Merisiers, Bât. 709, F-91191 Gif-sur-Yvette Cedex, France.
E-mail: pasb@lsce.saclay.cea.fr

monsoon rain into the Sahara (Joussaume et al. 1999). Part of this mismatch can be attributed to the omission of ocean response and feedbacks to insolation changes. Simulations of the 6 kyr BP climate where the atmosphere model is asynchronously (Kutzbach and Liu 1997) or synchronously (Hewitt and Mitchell 1998) coupled to a full dynamical ocean model indeed indicate that the ocean feedback enhances the increase of precipitation over Africa. This suggests that the whole energetic of the atmosphere is affected by the response of the ocean.

The aim of this paper is to investigate the impact of the ocean response to the 6 kyr BP insolation and the impact of its feedback on the seasonal cycle, and to analyze the ocean contribution to the equator-to-pole redistribution of heat, which was not addressed in previous studies. For this, we compare the climate change of two 6 kyr BP experiments. In the first one, the atmospheric model is synchronously coupled to an ocean model with no flux correction at the air–sea interface. The second is a PMIP-type experiment, where the atmosphere model is forced with prescribed modern SSTs. We designed our experiments so that the coupled control simulation is the reference for the two 6 kyr BP simulations. This appears to us to be the best way to investigate the role of the ocean. Our purpose here is not so much to assess the realism of our coupled experiment but rather to show where and how the response of the ocean influences the changes in monsoon circulation. We investigate the role of the ocean in the seasonal redistribution of heat from the equator to the poles by analyzing the relationship between insolation and the meridional heat transport computed directly by the coupled model. We also compare the change in atmosphere heat transport between the coupled and atmosphere-alone experiments.

In section 2, we present the coupled model and the climatology it simulates for present day. We then discuss in section 3 the 6 kyr BP climate with a focus on the change in the mean seasonal cycle and on the major differences in the summer African and Asian monsoons introduced by the reactive ocean. Section 4 is devoted to the analyses of the equator-to-pole heat transport.

2. Coupled simulation of the present-day climate

a. The coupled model

The coupled model is an improved version of the Institut Pierre Simon Laplace model, with no flux correction at the air–sea interface (Braconnot et al. 1997). The atmospheric component is version 5.3 of the Laboratoire de Météorologie Dynamique (LMD) atmospheric general circulation gridpoint model (Sadourny and Laval 1984). The resolution is 50 points in sine of the latitude, 64 points in longitude, and 11 vertical sigma levels. The oceanic component is the Océan Parallélisé model (Andrich et al. 1988; Madec and Imbard 1996) developed at Laboratoire d'Oceanographie Dynamique et de Climatologie (LODYC), with 92 points in longitude, 76 points in latitude, and 31 vertical levels, including 10 levels in the upper 100 m of the ocean. Sea ice cover is diagnostic, based on a test on SST in the oceanic model. It is then interpolated to the atmospheric grid where partial sea-ice cover is allowed. A fixed 3-m ice thickness is imposed to solve the thermodynamic equation and compute the sea-ice surface temperature. The two models are coupled once a day using the Ocean–Atmosphere–Soil Interface System coupler (Terray et al. 1995) developed at the Centre Européen de Recherche et de Formation Avancée en Calcul Scientifique (CERFACS).

The first simulations with that model exhibited a warm drift, most of which has been attributed to the energy imbalance of version 5.3 of the LMD model at the top of the atmosphere (Braconnot et al. 2000). Since then, several improvements have been included in the atmospheric model. Momentum and heat fluxes are now computed separately for sea ice and open water within icy grid boxes partly covered with sea-ice (Braconnot 1998). These changes are simpler than the double physic computation introduced by Grenier (1997) in another version of the LMD model. They affect only the vertical diffusion scheme between the first vertical level of the model and the surface, as in Grötzner et al. (1995). Following Krinner et al. (1997), a threshold value has been introduced to limit the bulk Richardson number used to compute surface fluxes. Also, the threshold on the diffusion coefficient in the overlaying boundary layer has been reduced. All these changes improve surface fluxes and correct a warm bias of the LMD5.3 model at high latitudes. Most of the reduction of the heat gain for the atmosphere–ocean system has been achieved by reducing the water droplet size from 20 to 10 μm, which increases cloud reflectivity. Within the Tropics, the simulation of the South Pacific convergence zone has been improved thanks to a reduction of the deep convection mixing. These differences in the atmospheric component introduce differences in the model sensitivity, so that PMIP-type experiments with this version of the model do not give exactly the same results in monsoon areas as the version used for PMIP (Masson and Joussaume 1997).

For the oceanic model, the main improvement compared to previous global coupled simulations (Braconnot et al. 1997; Guilyardi and Madec 1997) is the use of an isopycnal–diapycnal diffusion instead of the horizontal–vertical diffusion, like in recent global coupled simulations with the ocean at higher resolution (Barthelet et al. 1998; Guilyardi et al. 1999). There is no horizontal background diffusivity, but isopycnal slopes are horizontally smoothed to allow for a diffusion of gridpoint noise. Isopycnal slopes are limited to 1%. The isopycnal diffusion coefficient is 2000 $m^2 s^{-1}$. This parameterization reduces the drift after the initial spinup and maintains the zonal temperature gradients.

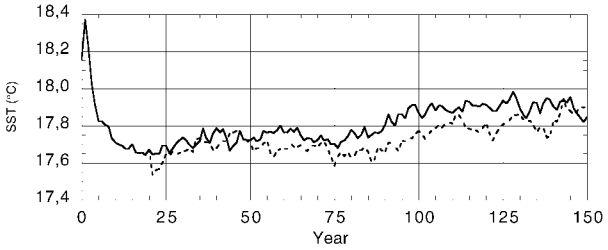

FIG. 1. Global annual-mean SST (°C) as a function of time for the modern and 6 kyr BP coupled simulations.

Braconnot et al. (1997) used a rather crude ''nearest neighbors'' interpolation scheme between models that did not ensure energy conservation. In the present experiment, the heat flux coming from an atmospheric grid box is divided between the underlying ocean grid boxes depending on their area. The local energy conservation is thus preserved. However, the global energy conservation is not exact because the two model coastlines do not match exactly. A small amount of energy is also lost in the simple sea-ice model where fixed heat flux of -2 W m^{-2} in the Arctic and -4 W m^{-2} in the Antarctic is imposed when an ocean grid box is frozen.

River and coastal runoff has also been included to close the hydrological cycle. Catchments for the 46 major rivers have been defined at the atmospheric model resolution, as well as their associated outflow. Corresponding river mouths have been defined on the ocean model grid. Coastal runoff is also taken into account and pours directly into the nearest coastal ocean grid boxes.

b. Present-day mean seasonal cycle

The control climate is a 150-yr simulation of the present-day climate with the coupled model described above (Fig. 1). The initial condition of the coupled integration for the atmosphere is 1 January of year 16 of an atmosphere-alone simulation forced with the mean seasonal cycle of Reynolds's (1988) SST and sea-ice cover. Prior to coupling, the ocean model has been spun up with annual mean forcing of wind stress (Hellerman and Rosenstein 1983), heat fluxes (Esbensen and Kushnir 1981), and water fluxes (Oberhüber 1988). This 10-yr spinup ensures a dynamic spinup of the circulation. It is too short to significantly change the thermohaline structure, which remains close to those of the Levitus atlas (Levitus 1982).

Starting from this initial state, the coupled model adjusts rapidly. After 20 yr of global cooling, the simulation is stable with a global mean SST of 17.8°C (Fig. 1). The drift is 0.2°C century^{-1} for the SST and less than 0.04°C century^{-1} for the global oceanic temperature. It is less than 0.01°C century^{-1} below 800-m depth. At the ocean surface and at the top of the atmosphere heat flux imbalance does not exceed 0.5 W m^{-2} in global average.

The annual-mean surface temperature shares most features of Reynolds's (1988) climatology (Fig. 2). However, the simulation exhibits a cold bias in tropical areas, reaching 4°C in the West Pacific warm pool and in the Sargasso Sea. A comparison (not shown) with heat fluxes estimated from the Earth Radiation Budget Experiment (ERBE; Barkstrom 1984) at the top of the atmosphere (TOA) suggests that this cold bias is the result of a smaller than observed heat absorption of about 40 W m^{-2} for the ocean–atmosphere system within the Tropics. During winter, it results mainly from an underestimation of the absorbed solar radiation at TOA. During summer most of the difference with ERBE arises from a too large emission of longwave radiation to space. In middle and high latitudes, on the other hand, SSTs are better reproduced. However, the system absorbs too much shortwave radiation in these regions, which yields an excessive surface summer warming amplified by a lack of sea-ice cover. In the Southern Ocean, sea-ice has vanished at all seasons except in small areas. In the Arctic the seasonal cycle of sea-ice is better reproduced, even though the sea ice cover of 11.7 km $\times$ 10^6 km built during NH winter is underestimated when compared to the 13.5 km $\times$ 10^6 km reported by Gloersen and Campbell (1991).

The meridional vertical slice of the zonally averaged ocean temperature (Fig. 3) shows that tropical cooling is limited to the first upper meters of the ocean and that the W-shape of the thermocline is reproduced. Below the thermocline, the ocean is warmer than in the observations, reflecting a too weak temperature gradient. Consistent with the smoother equator-to-pole SST and ocean heat content gradients, the equator-to-pole heat transport by the ocean (Fig. 4) is underestimated compared to indirect estimations from reanalyses (Keith 1995; Trenberth and Salomon 1994). North of 24°N the southward transport of North Atlantic Deep Water is less than 7 Sv and is not deeper than 2000 m, whereas according to Roemmich and Wunch (1985), it should reach about 20 Sv (Sv $\equiv$ 10^6 m^3 s^{-1}) down to 4500 m. Forced ocean experiments run to equilibrium exhibit a sharper equatorial thermocline and the ocean heat transport reaches 1.4 PW.

The atmospheric meridional heat transport (Fig. 4) is in good agreement with estimates from atmosphere reanalyses (Keith 1995). Atmospheric Hadley cells are well reproduced, whereas Ferrel and polar cells have a smaller than observed intensity (not shown). The total heat transport, sum of the ocean and atmosphere contributions, is smaller than the one derived from ERBE fluxes at TOA by about 1 PW.

Precipitation for June–August (JJA) gives an idea as to how the modern summer monsoon is simulated (Fig. 5c). For comparison, two climatologies are also plotted (Figs. 5a and 5b), as well as precipitation produced by the atmospheric component of the model when forced with climatological SST and sea-ice cover (Fig. 5d). The basic features of the monsoon flow are present, but the con-

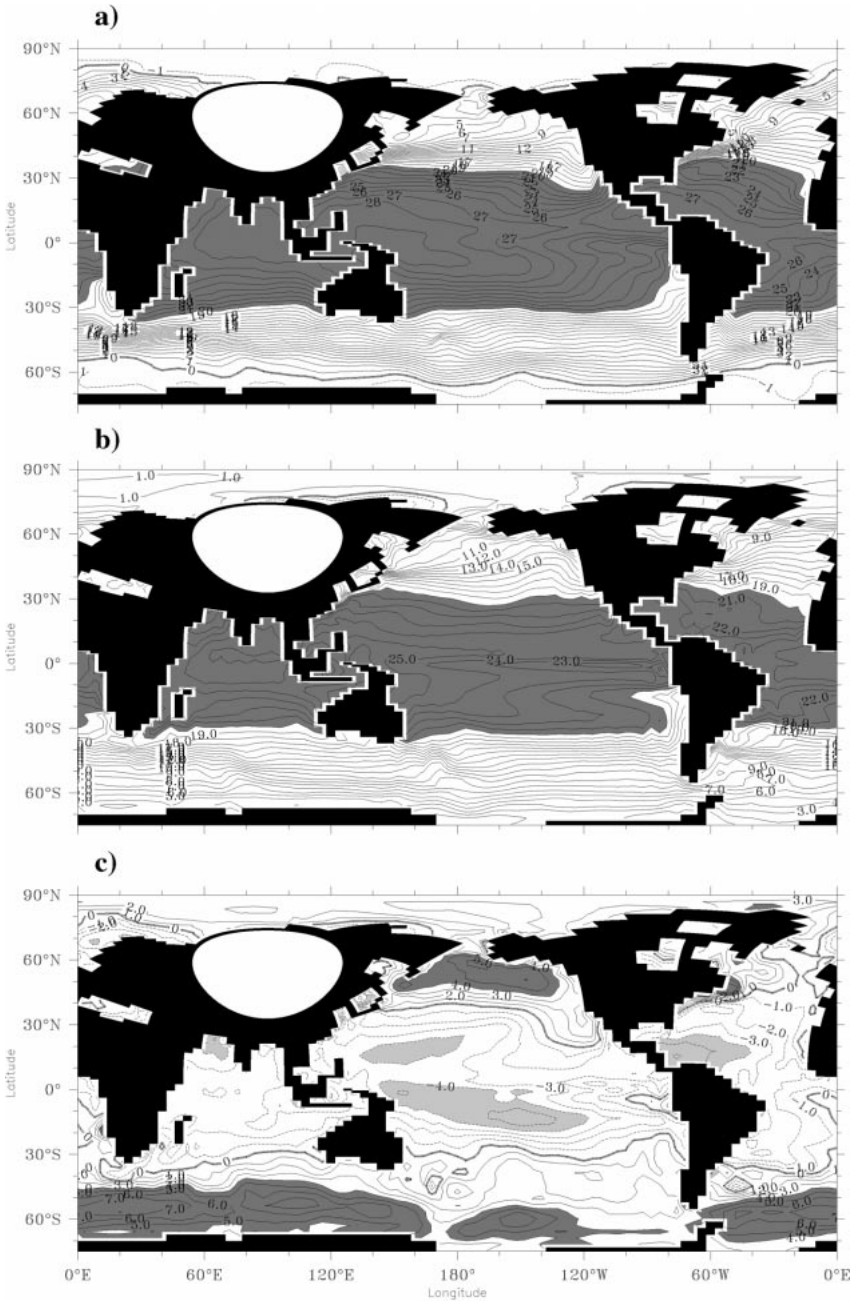

FIG. 2. Annual-mean SST for (a) Reynolds's (1988) climatology, and (b) the coupled modern simulation. Regions warmer than 20°C are shaded. (c) Difference between (b) and (a). Heavy gray (light gray) stands for differences exceeding 4°C (−4°C). Contour interval is 1°C for the three maps.

vergence zone is too active in Southeast Asia, and the north of India is too dry. The Intertropical convergence zone (ITCZ) is located too far north in Africa, with a maximum of precipitation around 12°N instead of the 10°N reported in the observations or in the atmosphere alone experiment. We attribute this northward shift to the cold SST simulated in the equatorial Atlantic. Despite this shift the precipitation features share most of the characteristics of uncoupled simulations (Fig. 5d) and fall among those produced by Atmospheric Modelling Intercomparison Project runs (Gadgil and Sajani 1998).

3. Simulations of the 6 kyr BP climate

a. Boundary conditions and simulations

The coupled simulation of the 6 kyr BP climate is 150 yr long and starts on 1 January of year 21 of the

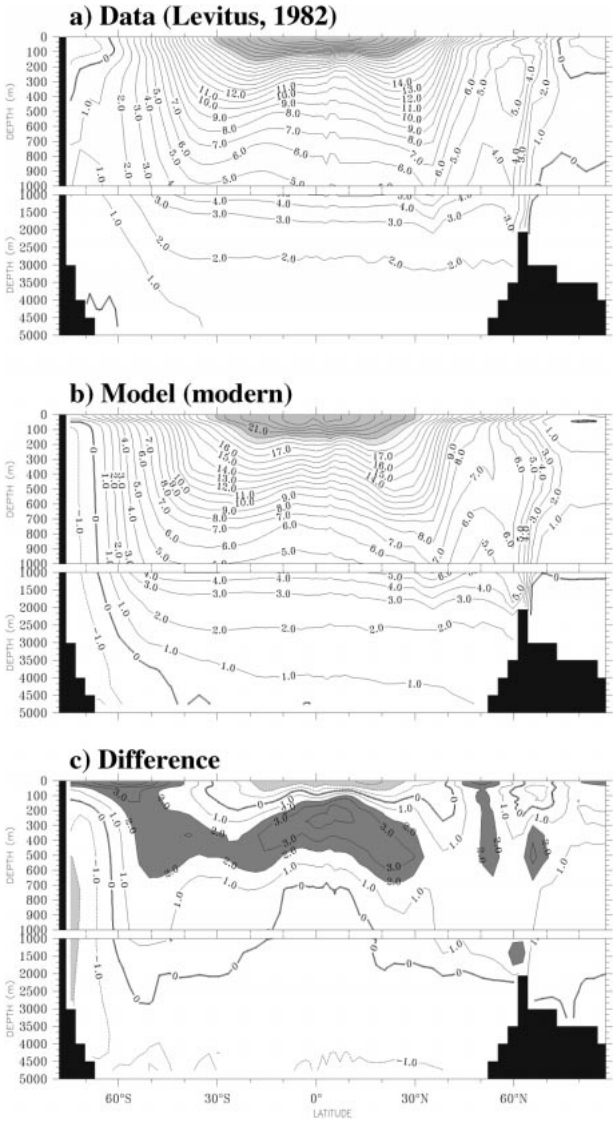

FIG. 3. Vertical slice of the annual zonally averaged temperature (°C) for (a) observations from Levitus atlas (Levitus 1982) and (b) the coupled modern simulation. Values warmer than 20°C are shaded. (c) Difference between (b) and (a). Heavy gray (light gray) stands for differences exceeding 2°C (−2°C). Contour interval is 1°C for the three panels.

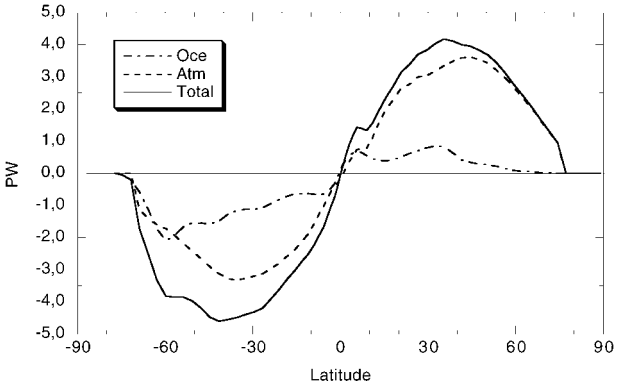

FIG. 4. Meridional heat transport (PW) in the ocean–atmosphere system (heavy solid line), in the atmosphere (solid line), and in the ocean (dashed–dotted line).

control simulation, at the end of the adjustment period (Fig. 1). The CO_2 level is kept to the value of the control experiment, as in Hewitt and Mitchell (1998), to avoid the long-term adjustment that would otherwise be needed to bring the deep ocean to equilibrium. Therefore, the only difference in boundary condition with the control simulation is the orbital configuration. Following PMIP recommendations (Joussaume and Taylor 1995), orbital parameters (Table 1) have been derived from Berger (1978), and the vernal equinox is fixed on 21 March at noon. The surface ocean adjusts very rapidly to the change in insolation and this simulation is quite stable (Fig. 1). The whole ocean drifts slightly, but at a rate similar to the one of the control experiment.

To compare the coupled simulation for 6 kyr BP with a PMIP-type simulation, we have also performed an atmosphere-alone simulation with the LMD5.3 model. However, the modern climate simulated using the coupled model differs in some aspects with the modern climate simulated with the atmospheric component when forced with observed SST and sea-ice cover. The basic state of the model may affect the model response to insolation change. Results of PMIP show that the location of the 6 kyr BP difference in precipitation in North Africa is a function of the location of the rainbelt of the control simulation (Joussaume et al. 1999). To avoid any bias that could arise from differences between modern climatology and modern SST simulated by the coupled model, we prescribed daily SST and sea-ice cover simulated by the control coupled simulation between year 80 and 100 to the 6 kyr BP atmosphere-alone simulation. With this methodology, the control coupled experiment is the reference for the two 6 kyr BP experiments.

The mean seasonal cycle of the atmosphere-alone experiment is obtained by averaging the last 20 yr of the simulation. The procedure we used requires the mean seasonal cycle for the control coupled experiment be computed from year 80 to 100. The coupled 6 kyr BP simulation the mean seasonal cycle also corresponds to a 20-yr average estimated from years 80 to 100. Since the model drifts in both coupled simulations are similar, this ensures a comparable level in the drift.

Only robust features of the climate change will be discussed in the following. We have checked that they do not depend on the averaging period by comparing results obtained from different 20-yr periods. We also use a modern calendar for month definition at 6 kyr BP rather than a more appropriate calendar based on celestial longitudes (Joussaume and Braconnot 1997). The reason is that this type of calendar was not introduced in the ocean model, for which only monthly values are

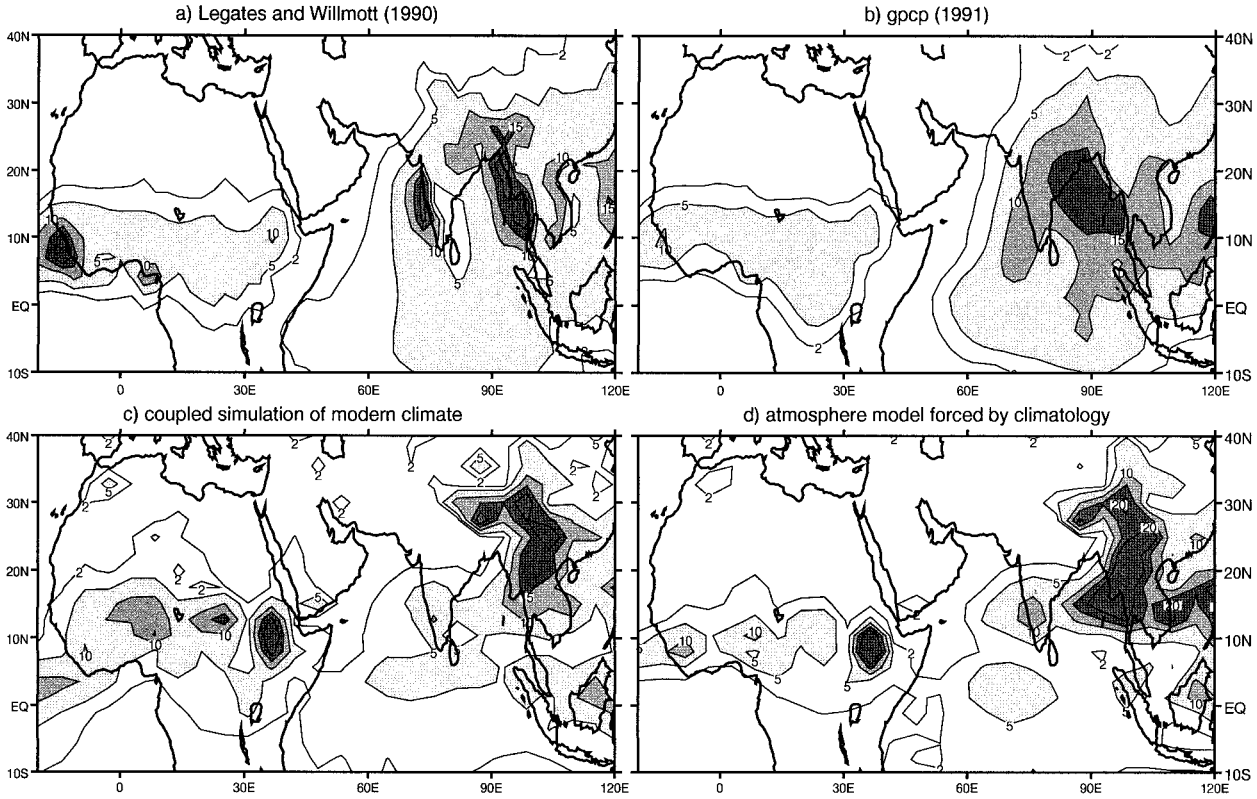

FIG. 5. JJA precipitation for Asia and Africa as inferred from (a) Legate and Willmott's (1990) climatology, (b) the climatology of the Global Precipitation Climatology Project (Janowiak and Arkin 1991), (c) the coupled simulation of the modern climate, and (d) a simulation with the atmospheric component of the coupled model forced with observed climatology of SST and sea-ice cover. Isolines 2, 5, 10, 15, and 20 mm day^{-1} are plotted. Values larger than 5 mm day^{-1} are shaded.

stored. With the modern calendar we arbitrarily damped the simulated changes in autumn.

b. Large-scale features of simulated 6 kyr BP climate

The 6 kyr BP orbital configuration leads to an increase of the seasonal cycle of the incoming solar radiation (insolation) at TOA in the NH and a decrease in the SH (Fig. 6a). As expected from this change in insolation, the seasonal cycle of surface temperature, defined here as the warmest month temperature minus the coldest month temperature, is enhanced in the NH (Fig. 7).

The gross features of the change are similar for the coupled and atmosphere-alone simulations, but the amplification of the seasonal cycle over land is of smaller magnitude for the coupled simulation. Over the ocean, the largest changes occur in the Atlantic where they exceed 1°C in a few places. In the Arctic region differences between the coupled and atmosphere-alone simulations arise mainly from a change in sea-ice cover. Figure 7c shows that the seasonal response can be of reverse sign between the two types of experiments over continental regions like North America, Europe, the Pacific coast of Asia, West Africa, and the northeast of South America. We can consider the 6 kyr BP climate change as the sum of the response of climate to insolation when the ocean does not vary (atmosphere-alone simulation) and of the feedbacks introduced by the response of the ocean to insolation (coupled minus atmosphere-alone simulation). Since the control simulation is the same for both the coupled and the atmosphere-alone 6 kyr BP simulations, no other factor is to be accounted for to obtain a pure factor separation (Stein and Alpert 1993). Using this separation, we can estimate that the ocean accounts for more that 75% of the simulated change in these regions, which stresses the large impact ocean variations have on these regions.

The ocean response also introduces a slight shift in the timing of the seasonal cycle. This delay was already noted by Kutzbach and Gallimore (1988) and Mitchell et al. (1988) in simulation of 9 kyr BP with an atmospheric model coupled to a slab-ocean model, and more

TABLE 1. Values of Earth's orbital parameters for the 6 kyr BP simulations.

Orbital parameters	Present day	4.1 kyr BP
Eccentricity	0.016724	0.018682
Axial tilt (°)	4.2	4.4
Perihelion − 180° (°)	4.3	4.5

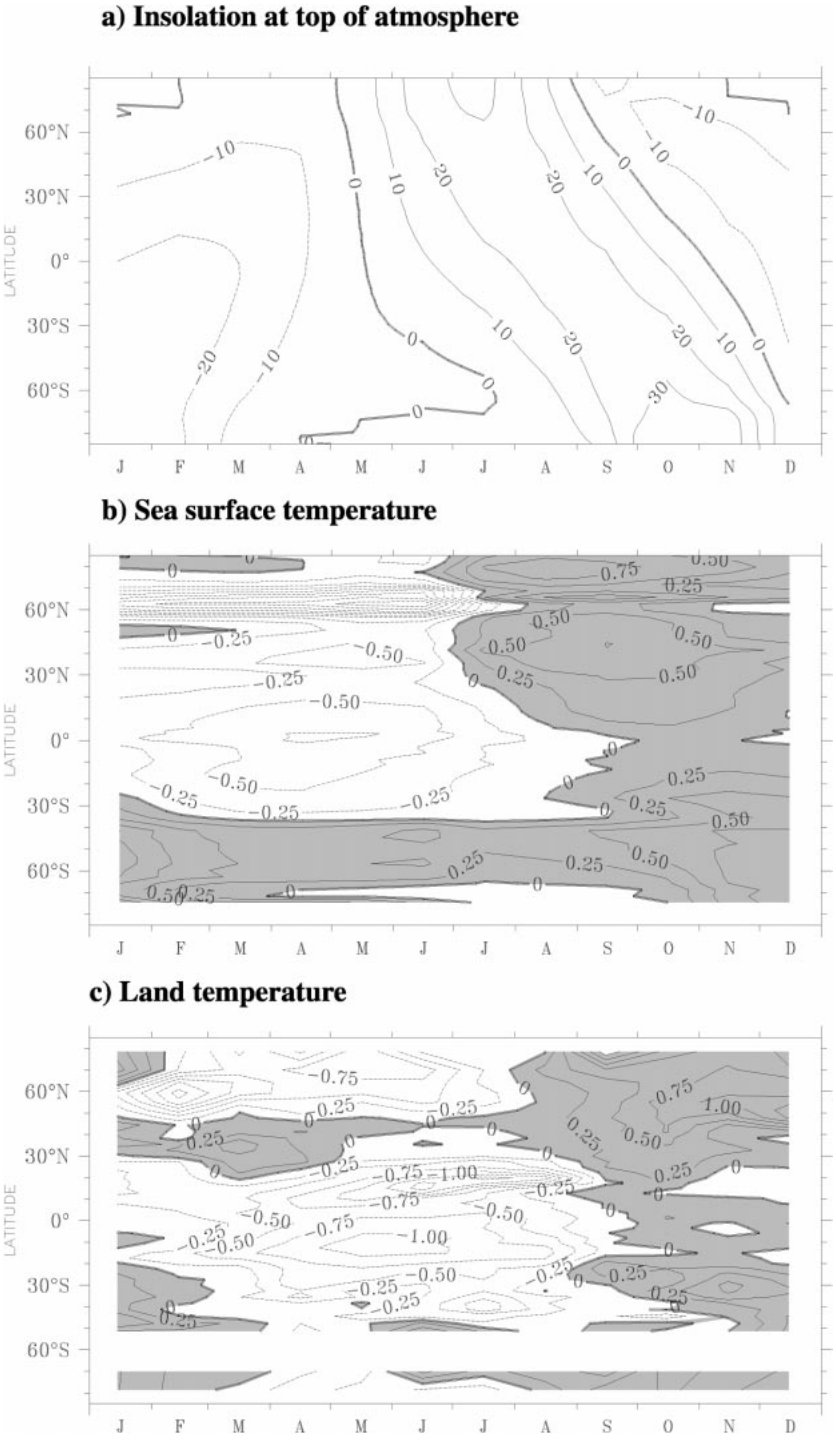

FIG. 6. (a) The 6 kyr BP change in incoming solar radiation at the top of the atmosphere, (b) 6 kyr BP change in SST, and (c) difference between the 6 kyr BP land surface temperature simulated by the coupled and atmosphere-alone simulations, zonally averaged and plotted as a function of months. In (a) the contour interval is 10 W m^{-2}. In (b) and (c) the contour interval is 0.25 °C and positive values are shaded.

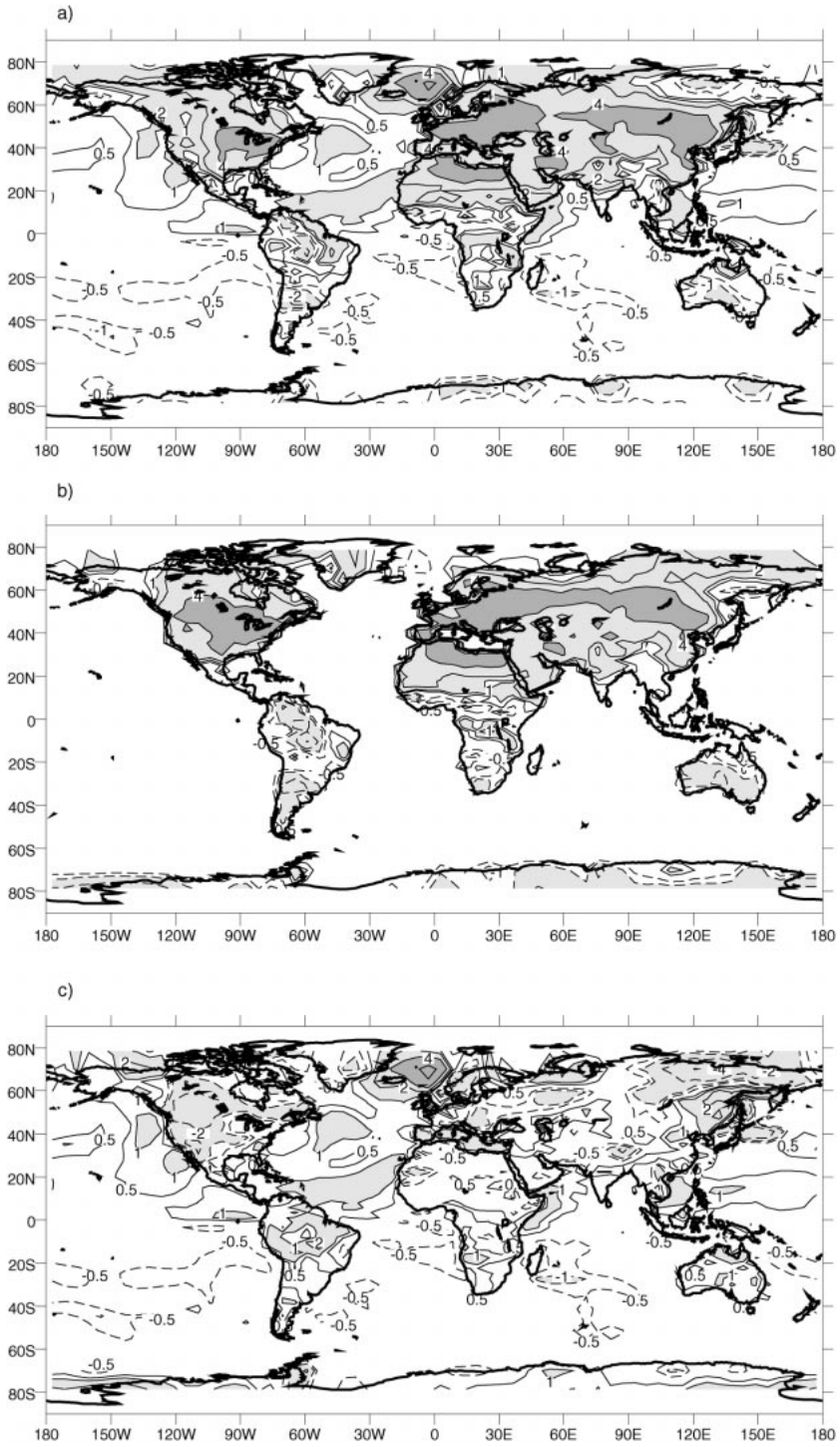

FIG. 7. Change in the magnitude of the surface temperature seasonal cycle (defined as the warmest month temperature minus the coldest month temperature for (a) the coupled 6 kyr BP simulation, (b) the forced atmospheric 6 kyr BP simulation, and (c) the difference between the 6 kyr BP coupled and atmosphere-alone simulations.

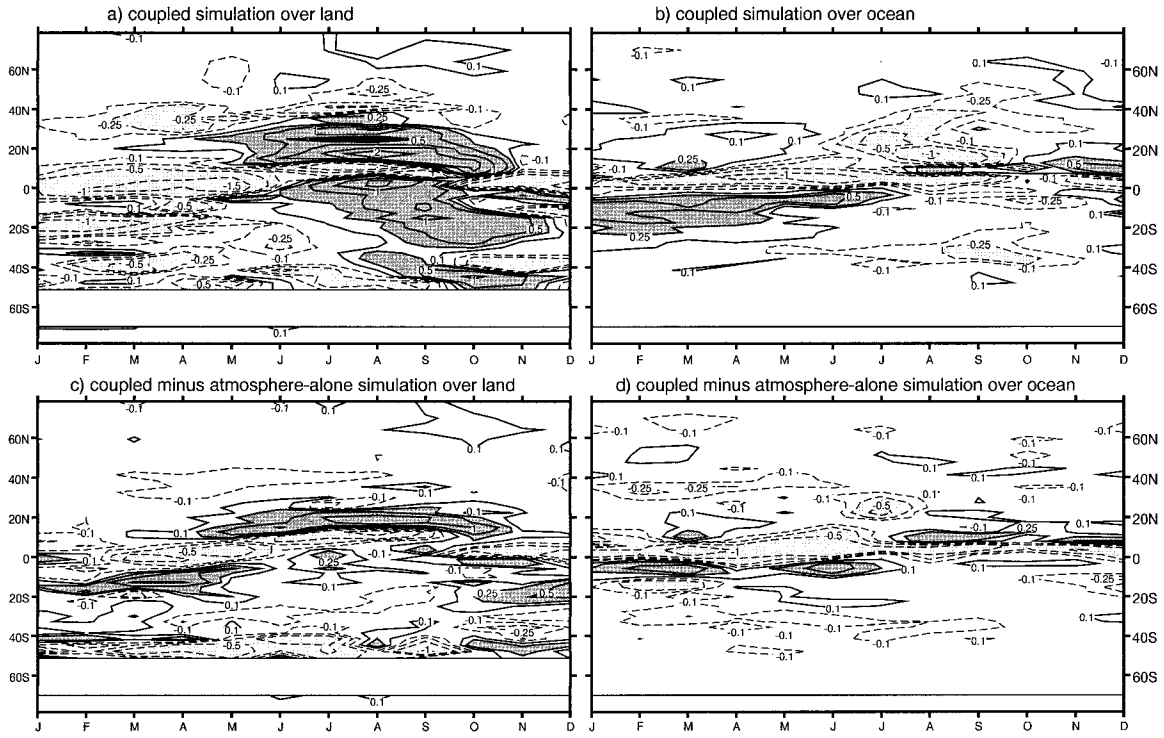

FIG. 8. The 6 kyr BP change in precipitation zonally averaged for (a) the coupled simulation over land, (b) the coupled simulation over the ocean, (c) the difference between the coupled and the atmosphere-alone simulations over land, and (d) the difference between the coupled and atmosphere-alone simulations over the ocean. Isolines ± 0.1, 0.25, 0.5, 1, 2, and 3 mm day^{-1} are plotted. Negative values smaller that -0.1 mm day^{-1} are dotted and positive values larger than 0.25 mm day^{-1} are shaded and are considered to be significant.

recently by Hewitt and Mitchell (1998) in a fully coupled experiment of the 6 kyr BP climate. In our model, although insolation is most reduced in January–February within the Tropics (Fig. 6a), the maximum cooling over the ocean occurs only 2–3 months later (Fig. 6b). The maximum warming in middle latitudes also lags by 2 months the insolation forcing. In the high latitudes of the NH, the warming follows more closely the insolation because the melting of sea-ice begins nearly in phase with the change in solar radiation, which reduces the surface albedo and favors the ocean warming.

Interestingly, a slight shift in the timing of the temperature change over land can also be depicted from the zonal mean difference between the coupled and atmosphere-alone simulations of 6 kyr BP (Fig. 6c) in spring and autumn. These differences are larger than differences between two 20-yr means (0.1°–0.2°C depending of latitude and seasons) of the control coupled simulation. Note that this pattern is independent of any choice of calendar (Joussaume and Braconnot 1997).

Following the changes in temperature, the land–sea pressure gradient is reduced in NH winter and increased in NH summer, increasing the seasonal march of the ITCZ. Therefore, the ITCZ is located farther south over the ocean in winter, which is characterized by the plus (minus) structure over the ocean (Fig. 8b), and farther north over land in summer, which is characterized by the plus (minus) structure over land (Fig. 8a). The comparison between the coupled and atmosphere-alone simulations shows that the shift of the position of the rainbelt is more pronounced when the ocean is active (Figs. 8c and 8d). In summer, the inland penetration of the rainbelt also started one month earlier (Fig. 8c). In agreement with the maintenance of warming over the ocean and the continent in late spring, the southward retreat of the rain belt is delayed by 1 month both over land and over the ocean (Figs. 8c and 8d).

Figure 8 also clearly shows that the role of the ocean on the hydrological cycle is not negligible since the differences between the two 6 kyr BP simulations are of the same order of magnitude as the 6 kyr BP precipitation change in most seasons. The largest impact is located within the Tropics and is the signature of changes in the Hadley–Walker circulation.

c. Response of the Indian and African monsoons

In NH summer, the zonal-mean change in precipitation over land reflects the changes in the monsoon circulation (Kutzbach et al. 1993; Hewitt and Mitchell 1996; Hall and Valdes 1997; Masson and Joussaume 1997; Joussaume et al. 1999). Monsoon activity can be deduced from the net longwave radiation at the top of the atmosphere. The signature is an enhanced trapping

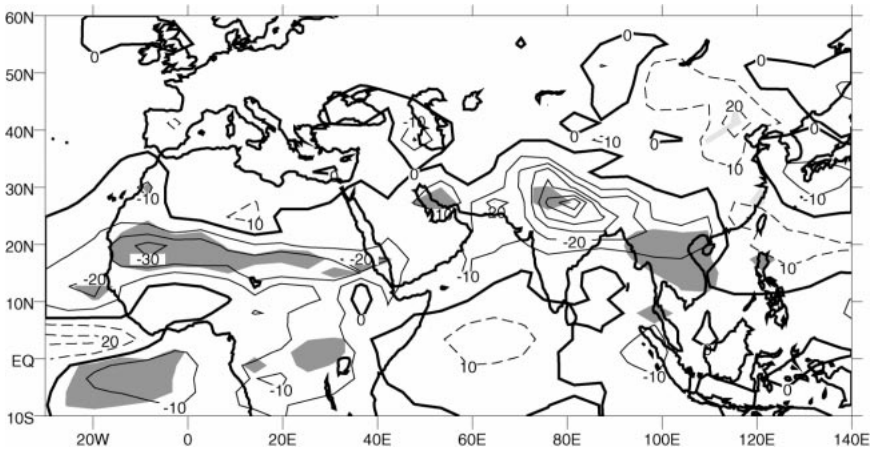

FIG. 9. JJA change in longwave radiation at TOA for the 6 kyr BP coupled simulation. Shading indicates regions where the differences between the coupled and atmosphere-alone simulations exceed 10 W m^{-2}, with light (heavy) gray for negative (positive) values.

of longwave radiation from Africa to India and Southeast Asia (Fig. 9)

Even though the summer continental warming is smaller in the coupled simulation, the airmass redistribution between a colder ocean and the continent leads to a deeper monsoon low over Eurasia and North Africa (Fig. 10). Major differences between the two simulations are located over central Eurasia and extend from north India to Egypt, near the Pacific coast between 40° and 50°N and in West and northwest Africa. This pattern reflects differences in the structures of the continental warming (not shown). Following the basic dynamics of tropical regions (Wang et al. 1996), a maximum upward velocity is located to the southeast of each pressure minimum, which explains the increased convection between the coupled and atmosphere-alone simulations north of India, over Arabia and East Africa (Fig. 9).

In Southeast Asia the response of the monsoon circulation differs between the coupled and atmosphere-alone simulations (Figs. 9 and 10). When the ocean varies, the pressure deepening over land is associated with a pressure rising over the West Pacific. This feature induces a convergence of moisture from the Pacific and the Indian Ocean toward Southeast Asia and increases the convection in this region.

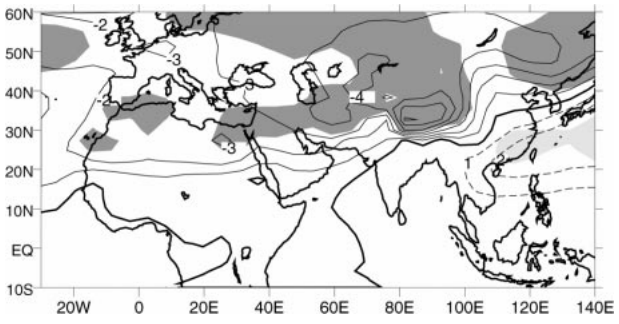

FIG. 10. JJA change in sea level pressure for the 6 kyr BP coupled simulation. Shading indicates regions where the differences between the coupled and atmosphere-alone simulations exceed 1 hPa with light (heavy) gray for negative (positive) values.

West Africa is also a region where significant differences are found between the two types of experiment. One reason is that the Atlantic Ocean has the largest response to insolation (Fig. 6). In summer the SST change exhibits a gradient of temperature across 15°N with colder temperature to the south and warmer temperature to the north. This feature shares some similarities with the structure of Atlantic SST that are believed to have a large positive impact on Sahel rainfall (Palmer 1986; Folland et al. 1986; Lamb and Peppler 1992; Fontaine and Janicot 1996). The 6 kyr BP SST changes simulated with the coupled model are small, but the change in SST gradient they create in the Atlantic Ocean is larger than the change involved in West African modern variability. The minimum of pressure in West Africa becomes deeper in late summer. It generates a local cyclonic circulation that favors precipitation in the west (not shown).

Precipitation zonally averaged from the West African coast to 30°E (Fig. 11) indicates that the northern limit of the modern rain belt is located at 20°N, where advection (estimated in Fig. 11 from precipitation minus evaporation) falls to zero. As discussed in Braconnot et al. (1997), this limit coincides with the location of the maximum of surface temperature, which is also the location of the minimum of the thermally forced pressure low over the Sahara. Note that the rainfall amount is larger than it should be north of 20°N. This is a common model drawback (Braconnot et al. 1997). Figure 13a shows that this excess is due to local recycling. It is a local feature and does not seem to impact on the climate change.

At 6 kyr BP the warming north of 20°N is sufficient to shift northward the maximum of temperature and monsoon rains penetrate farther north (Fig. 11a). Most

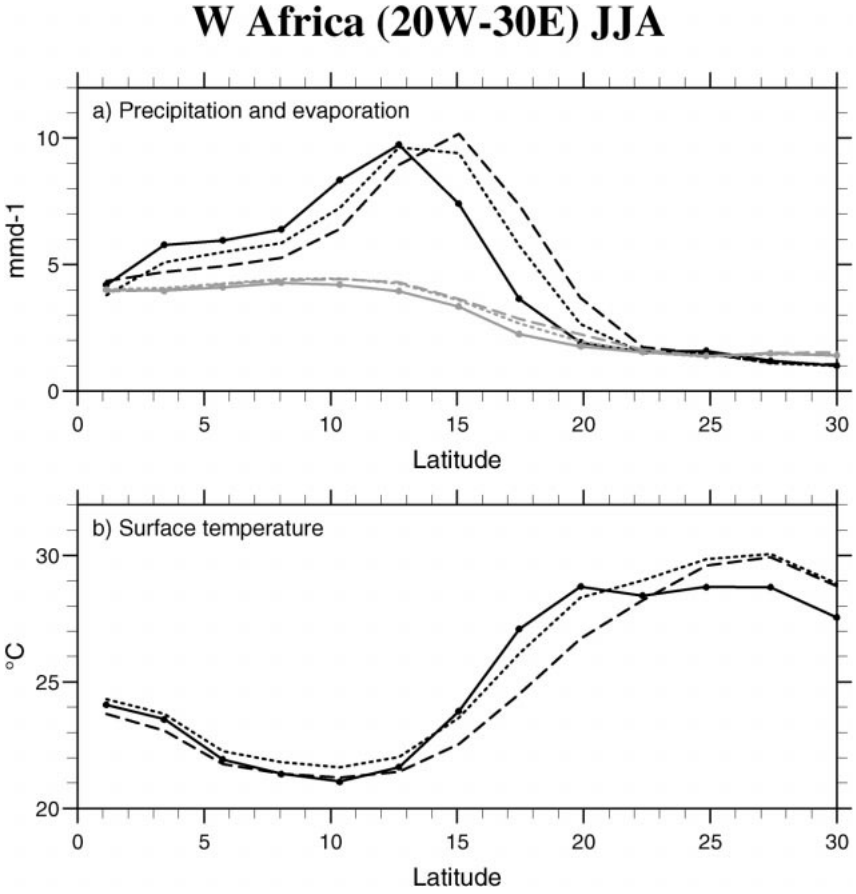

FIG. 11. JJA (a) precipitation and evaporation, (b) surface temperature zonally averaged over West Africa between 20°W and 30°E for the control simulation (solid line), the 6 kyr BP atmosphere-alone simulation (dotted line), and the 6 kyr BP coupled simulation (dashed line).

of the change in the moisture supply results from the change in water vapor advection (Fig. 11a). Between 15° and 22°N the change in precipitation is about twice larger in the coupled experiment, and the northernmost limit of the rainbelt is shifted by about 1.5° farther north. Results of the coupled simulation are in better agreement with paleoclimate indicators (Jolly et al. 1998) than PMIP simulations (Joussaume et al. 1999). However, the northward penetration of monsoon rain into the Sahara is not sufficient to match the steppic vegetation indicated by pollen data up to at least 23°N.

4. Heat fluxes and meridional heat transport

Monsoon activity is one of the key mechanisms sustaining the Hadley circulation and the export of heat from the equator to tropical regions through latent heat release. The more vigorous 6 kyr BP summer monsoon is a way to transfer the additional insolation heating resulting from the change in Earth's orbital parameters from the NH to the SH (Masson and Joussaume 1997). Surface temperature and precipitation changes at 6 kyr BP zonally averaged over the globe (Figs. 6 and 8) suggest that the equator-to-pole redistribution of heat is not only affected in summer but throughout the year.

a. Atmospheric and oceanic contributions to changes in meridional heat transport

Seasonal variations of the latitudinal distribution of the 6 kyr BP change in net heat fluxes at TOA (netTOA) follow the insolation pattern (Fig. 6a), but with a smaller magnitude (Fig. 12a). It is also more noisy, because it reflects adjustments occurring within the ocean–atmosphere system.

As illustrated for February and July in Fig. 13a and 13c, the change in netTOA (ΔnetTOA) can be decomposed into:

$$\Delta\text{netTOA} = \text{SW forcing} + (\Delta\text{netSW} - \text{SW forcing}) + \Delta\text{netLW},$$

where ΔnetSW stands for the change in net downward heating by solar radiation, ΔnetLW for the change in net upward cooling by infrared radiation, and SW forcing is the shortwave forcing, defined as the net short-

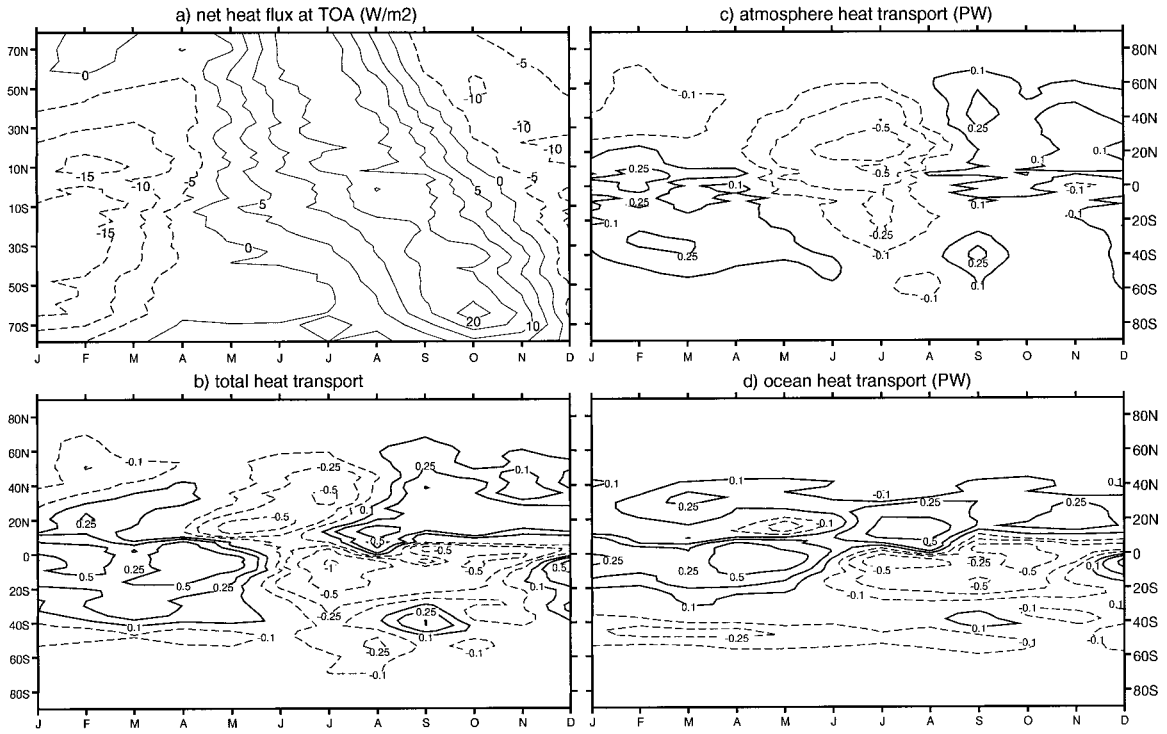

FIG. 12. Seasonal evolution in zonal mean of the change in (a) net heat flux at TOA (W m^{-2}), (b) total equator-to-pole heat transport (sum of the ocean and atmosphere heat transports; PW), (c) atmosphere heat transport (PW), and (d) ocean heat transport (PW), extracted from the coupled experiment. For the heat transports, values larger than 0.1 PW exceed the differences between two 20-yr means of the control simulation and are considered to be significant.

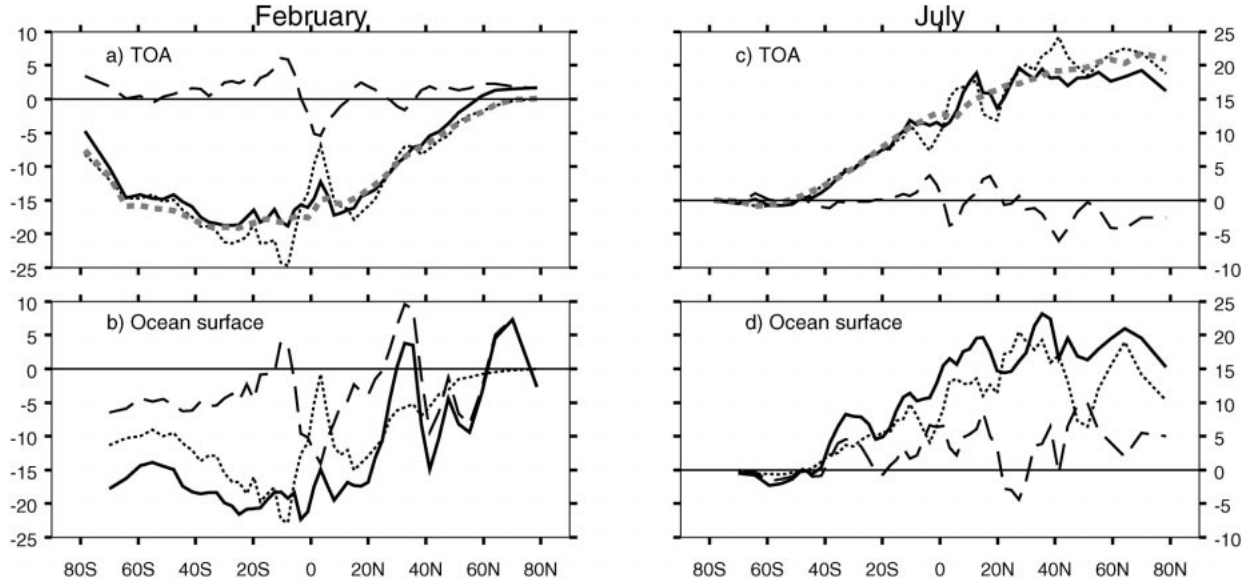

FIG. 13. Zonal average (W m^{-2}) for Feb (left) and Jul (right) of the 6 kyr BP changes in (a) and (c) heat fluxes at TOA, including the SW forcing (gray dotted line), defined as $(1 - \alpha)\Delta SW_i$, where α is the modern planetary albedo and ΔSW_i is the change in insolation; SW radiation (thin dotted line); LW radiation (thin dashed line); and net heat flux (SW + LW; dark solid line). (b) and (d) Heat fluxes at the ocean surface, including net SW (thin dotted line), net nonsolar flux (thin dashed line), and net heat flux (solid line).

wave radiation difference at TOA between 6 kyr BP and present with the assumption that the planetary albedo does not change between the two periods [SW forcing = $(1 - \alpha)\Delta SW_i$ where α is the modern planetary albedo and ΔSW_i is the change in insolation]. Indeed, the SW forcing caused by the 6 kyr BP insolation is not directly the insolation change, because the planetary albedo reflects back to space part of the incident solar radiation. The SW forcing can vary from one model to the other depending on clouds and surface properties. For our coupled model, the 6 kyr BP SW forcing is maximum between 10°S and 40°S in February and north of 40°N in July (Fig. 13), following the insolation change. The difference between the SW forcing and the net SW flux at TOA results from cloud and water vapor feedbacks. For example, within 20°S and 20°N the southward shift of the ITCZ (Fig. 8) can be clearly seen in February from the plus/minus structure on the net SW curve (Fig. 13a). For most latitudes and seasons, the change in outgoing longwave radiation tends to counterbalance the difference between the net SW and the SW forcing (Figs. 15a and 15c). As a result, the change in netTOA is not very different from the SW forcing (Fig. 15).

Similarly, the net heat flux at the ocean surface can be decomposed into the net solar flux and the net nonsolar flux (Fig. 13), the latter including the longwave, the sensible, and the latent heat fluxes. For most latitudes, the change in nonsolar heat flux amplifies the change in net solar heat flux, both in February and July (Figs. 13b and 13d).

These changes reflect the redistribution of heat sources and sinks for the ocean–atmosphere system between 6 kyr BP and present (Fig. 12a). Under equilibrium climates (i.e., zero netTOA in global annual mean), the annual-mean net TOA is balanced by the divergence of the change in the annual-mean meridional heat transport. Since our coupled simulations drift slightly, these two terms do not match perfectly. However, the residual, which represents an annual-mean heat storage in the system, can be neglected in the analysis below, because the model drift is small and similar in the two coupled experiments. At the seasonal timescale we are looking at, the seasonal divergence of the meridional heat transport does not necessarily balance the latitudinal change in netTOA. The seasonal heat storage has to be accounted for.

In our case, for example, the changes in total heat transport, computed here as the sum of the atmospheric and oceanic heat transports, nearly balance for each month the change in netTOA in the NH (Figs. 12a and 12b). This is not the case in the SH and for most seasons within the Tropics. Indeed, from January to March there is less heat entering the system at TOA from 30°S to 10°N at 6 kyr BP, which should reduce the equator-to-pole heat transport. The change in heat transport rather exhibits a northward component at that time. The same occurs in autumn when the additional heating in the SH should favor a northward interhemispheric heat transport. The simulated total heat transport is directed to the south in the SH. The analysis of the atmosphere and ocean contributions to the 6 kyr BP change in total heat transport (Figs. 12c and 12d) shows that the ocean is responsible for this feature. Indeed, the change in the atmospheric transport (Fig. 12c) is quite consistent with the change in netTOA.

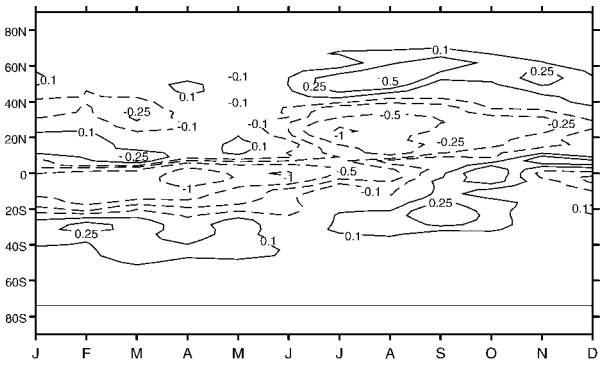

FIG. 14. Seasonal evolution (zonally averaged over ocean grid points) of the change in latent heat transport (PW) in the atmosphere, computed using results of the coupled experiment.

The ocean pattern (Fig. 12d) does not match a straightforward response to insolation or to ocean surface fluxes. Indeed, to balance the surface fluxes (Fig. 13), one would expect the change in ocean heat transport to exhibit a southward component both in the NH in winter and across the equator in summer. Throughout the year major changes in ocean heat transport are located within the Tropics (Fig. 12d). In these regions, the meridional oceanic heat transport appears to be anticorrelated with the atmospheric transport of latent heat zonally averaged over ocean grid points (Fig. 14). The latter is primarily due to low-level winds. The anticorrelation we find illustrates that the ocean heat transport mostly reflects the dynamic adjustment of the ocean to changes in wind forcing. Indeed the Ekman transport in the ocean is directed to right angle to the surface stress and to the right of it (left of it) in the NH (SH). In zonal average, the latent heat and Ekman transports are thus opposite in direction. The change in Ekman transport is dominant in equatorial regions. In extratropical regions, the heat storage in the ocean also constrains the equator-to-pole heat transport. During December–February, for example, the heat transport in the SH (Fig. 12d) is consistent with the changes in SST (Fig. 6b).

Figure 12 also shows that the ocean heat transport plays an important role in the redistribution of heat in the 6 kyr BP climate. Its role is even dominant in the SH and within the Tropics in spring and autumn. Note also that the change in ocean heat transport is directed to the north around 30°N throughout the year. The associated convergence reinforces the direct effect of the insolation forcing in summer and damps it in winter.

This explains why SST are larger at this latitude for all months compared to the surrounding latitudes.

b. Atmospheric heat transport in the coupled and atmosphere-alone 6 kyr BP simulations

Since the ocean contribution to the latitudinal redistribution of heat is not negligible, we may wonder what happens when the SST is not allowed to vary, like in the atmosphere-alone 6 kyr BP simulation. Even though the SSTs do not vary, heat fluxes at the ocean surface change according to insolation and cloud and water feedbacks. The corresponding change in seasonal ocean heat transport however cannot be computed, because the heat content of the ocean is not known. We then compare only the atmospheric transports.

We have designed our 6 kyr BP simulations in order to ensure that the coupled control experiment is the reference for both of them. The shortwave forcing is thus also the same. The netTOA difference between the two 6 kyr BP simulations then arises only from differences of internal feedbacks. As shown for the coupled simulations (Fig. 13), feedbacks are such that their impact on SW and LW nearly cancel, so that the change in netTOA resembles the SW forcing. This remains true for the atmosphere-alone experiment (Figs. 15a and 15e), and differences between the two experiments do not exceed 3 W m^{-2}. At the surface (including land and ocean grid points), heat fluxes are more different, and can even have an opposite sign, like north of 20°N in February (Fig. 15b), or between south of 60°S in July (Fig. 15g). Changes in the net heat budget for the moist atmosphere (Fig. 15c and 15h), computed as the difference between heat fluxes at TOA and at surface, are thus modified according to the surface response. Since the heat storage is negligible in the atmosphere, they are counterbalanced by changes in the atmospheric heat transport (Figs. 15d and 15i), which is achieved through dry static and latent heat transports (Fig. 15e and 15j).

The changes in the atmospheric meridional heat transport produced by the two 6 kyr BP experiments most differ in winter from 20° to 60°N. It is northward in the atmosphere-alone experiment, whereas its sign reverses across 30°N in the coupled experiment. In the latter, the 6 kyr BP change yields a heat convergence toward 30°N. Figure 15e shows that this is mainly due to differences in the dry static heat transport. This different behavior between the two experiments is consistent with the warmer temperatures simulated over land around 30°N at 6 kyr BP with the coupled model (Fig. 6c). The coupled and atmosphere-alone simulations also produce a different change in the meridional heat transport south of 20°S (Fig. 15d). In this region, both the dry static and latent heat transports contribute to the difference (Fig. 15e). Within the Tropics, changes in heat transport are similar in the two experiments, but Fig. 15e shows that compensations occur between the changes in dry static and latent heat transport associated with modifications of the Hadley circulation.

In NH summer, represented by July in Fig. 15, the atmosphere is also more efficient in redistributing the energy excess from middle latitudes to the Tropics when coupled to the ocean (Fig. 15i). Part of the difference is also due to the hydrological cycle through the moisture transport (Fig. 15j), whose changes have opposite direction between the coupled and atmosphere alone simulations. There is no clear signature of the change in the tropical circulation, mainly because in July there is a competition between a more active monsoon on the continent and a southward shift and less active ITCZ over the ocean.

The common feature between winter and summer is that the atmosphere transports less heat from the equator to the poles in the coupled experiments, because the ocean contributes to the equator-to-pole heat transport.

5. Conclusions

The role of the ocean in the 6 kyr BP climate is investigated by comparing results of two experiments: a no–flux corrected coupled ocean–atmosphere simulation and a simulation with the atmospheric model for which SSTs are kept to the modern ones. For these simulations, Earth's orbital parameters have been changed from their present values to those valid 6 kyr ago. The resulting change in insolation strengthens the seasonal cycle in the NH, and the summer African and Asian monsoon are more vigorous. This picture supports the main findings from different atmospheric models (Joussaume et al. 1999).

Our experimental design is such that 6 kyr BP changes simulated with the coupled model or with the atmosphere model can be directly compared. We suppress any bias in the comparison that would arise from a different control simulation by prescribing in the atmosphere-alone simulation SSTs and sea ice from the results of the control coupled simulation. Our results show that the hydrological cycle is more altered when the atmosphere is coupled to the ocean, and that the summer monsoon is more vigorous and penetrates farther north in the Sahara. The coupled experiment is in better agreement with paleodata over this region. The SST response lags the insolation forcing by 2–3 months. This delay has an impact on the timing of the monsoon change, which begins 1 month earlier because of colder SST and retreats more slowly in autumn in West Africa, when SSTs exhibit a gradient across 20°N with warmer SSTs to the north and colder SSTs to the south. In most coastal regions, the climate response is very different, and even of opposite sign between the two experiments, which stresses the role of the ocean in these areas. Most of these results are consistent with those Hewitt and Mitchell (1998) got with the coupled model of the Hadley Center. Kutzbach and Liu (1997) also found that the African monsoon penetrates farther inland in simula-

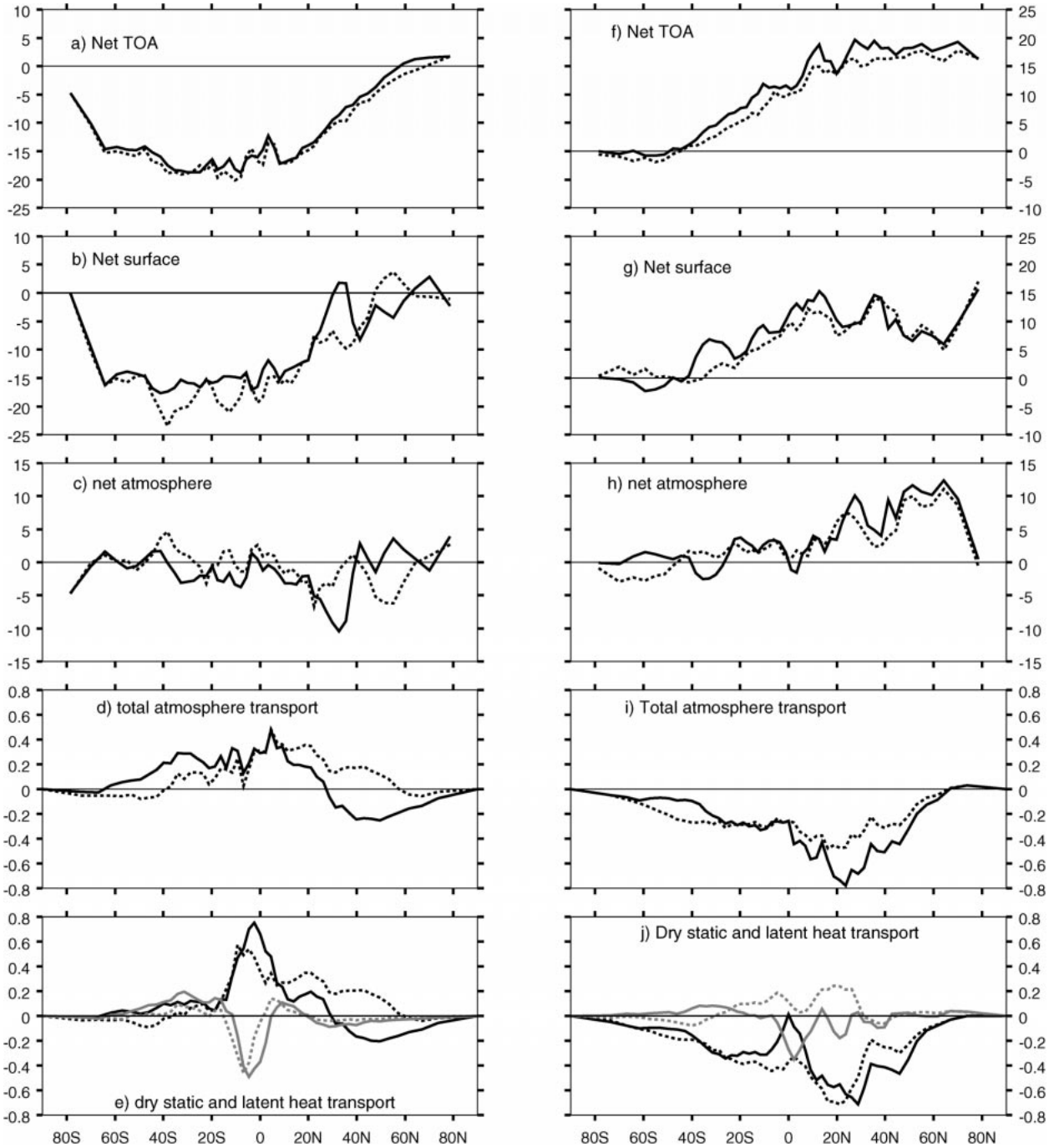

FIG. 15. The 6 kyr BP change in the atmosphere heat budget components for the coupled (solid line) and the atmosphere-alone (dashed line) simulations zonally averaged for Feb (left) and Jul (right). (a) and (e) Net heat flux at TOA (W m^{-2}); (b) and (f) net heat flux at the surface (W m^{-2}); (c) and (g) total heat transport (PW) by the atmosphere; and (d) and (h) dry static (black) and latent heat (gray) transports (PW).

tions in which the atmosphere model is asynchronously coupled to an ocean model.

We go one step further by analyzing the impact of the interactive ocean on the poleward heat transport. The 6 kyr BP insolation change creates seasonal perturbations of the zonal-mean solar forcing, which affect in turn the meridional heat transport, the role of which is to redistribute the energy excess from sources to sinks. Both the atmosphere and ocean heat transports participate in the redistribution of energy. From results of the coupled simulation, we show that the change in heat transport in the ocean is as large as the one of the at-

mosphere at most latitudes and seasons. The largest variations in the ocean occur in the Tropics where they do not follow changes in temperature or surface fluxes but the changes in the atmospheric Hadley circulation. The good correlation between the change in ocean heat transport and the change in the atmosphere transport of latent heat suggests a strong connection between surface wind and the ocean behavior and confirms that the Ekman transport plays a strong role in low latitudes (Trenberth and Salomon 1994).

Keeping the SSTs as in the control simulation in the 6 kyr BP atmosphere-alone experiment has also an impact on the atmospheric heat transport, because some of the feedbacks within the ocean–atmosphere system are different. Our results show that these differences cannot be detected from differences in the heat budget at the top of the atmosphere where compensation occurs between shortwave and longwave radiation. The coupled and atmosphere-alone simulations have almost the same change in net heat flux at TOA but with a different heat transport in the atmosphere. Our comparison also suggests that for some regions or seasons such as at 30°N, the heat transport plays a role as large as the insolation forcing in determining the temperature change in the ocean and also on land. This needs to be investigated further in order to understand the key factors controlling the SST changes and in particular how the north–south SST gradient in the Atlantic Ocean is created and maintained.

Other factors have been shown to have a profound impact on the response of the African monsoon. Simulations where vegetation change was prescribed (Kutzbach et al. 1996) or computed by asynchronously coupling the atmosphere model to a biome model (Claussen and Gayler 1997; Texier et al. 1997), show that vegetation feedbacks enhanced the insolation forcing. Lakes and wetlands induce also a source of moisture on the continent and contribute to reinforce the African monsoon (Coe and Bonan 1997). Ganopolski et al. (1998) with a simplified ocean–atmosphere–vegetation model found that ocean–vegetation feedbacks affect the meridional heat transport. We recently introduced vegetation feedback in our coupled simulations and showed synergistic interaction with ocean feedbacks in West Africa (Braconnot et al. 1999). These simulations show the role of the land–sea contrast in the 6 kyr BP climate change. We need now to understand better how this contrast impacts on the energy and water cycles between land and ocean.

Acknowledgments. We thank the LMD, the LODYC, and the CERFACS for, respectively, providing the atmosphere model, the ocean model, and the coupler. The new version of the coupled model benefits from discussions and interactive work with members of the Gaston group. We also thank D. Paillard and P. Yiou for their comments on the first version of the manuscript. The computer time was provided by the Commissariat à l'Energie Atomique. Drawings were performed using Vairmer, the software developed at CERFACS and VCS, developed at PCMDI. This work was supported by PNEDC and EEC under Contract ENV4-CT95-0075.

REFERENCES

Andrich, P., P. Delecluse, C. Levy, and G. Madec, 1988: A multitasked general circulation model of the ocean. *Proc. Fourth Int. Symp. on Science and Engineering on Cray Supercomputers,* Minneapolis, MN, Cray, Inc., 407–428.

Barkstrom, B. R., 1984: The Earth Radiation Budget Experiment (ERBE). *Bull. Amer. Meteor. Soc.,* **65,** 1170–1185.

Barthelet, P., and Coauthors, 1998: Simulations couplées globales des changements climatiques associés à une augmentation de la teneur atmosphérique en CO_2. *C. R. Acad. Sci. Paris,* **326,** 677–684.

Berger, A., 1978: Long term variation of daily insolation and Quaternary climatic changes. *J. Atmos. Sci.,* **35,** 2362–2367.

Braconnot, P., 1998: Tests de sensibilité avec le modèle d'atmosphère du LMD, en vue d'améliorer le couplage avec l'océan. Institut Pierre Simon Laplace Tech. Note 2, 39 pp. [Available online at http://www.ipsl.jussieu.fr/modelisation/liste-notes-tech.html]

——, O. Marti, and S. Joussaume, 1997: Adjustment and feedbacks in a global coupled ocean–atmosphere model. *Climate Dyn.,* **13,** 507–519.

——, S. Joussaume, O. Marti, and N. de Noblet, 1999: Synergistic feedbacks from ocean and vegetation on the African monsoon response to mid-Holocene insolation. *Geophys. Res. Lett.,* **26,** 2481–2484.

——, ——, N. de Noblet, and G. Ramstein, 2000: Mid-Holocene and Last Glacial Maximum African monsoon changes as simulated within the Paleoclimate Modeling Intercomparison Project. *Global Planet. Change,* in press.

Claussen, M., and V. Gayler, 1997: The greening of the Sahara during the mid-Holocene: Results of an interactive atmosphere-biome model. *Global Ecol. Biogeogr. Lett.,* **6,** 369–377.

Coe, M. T., and G. B. Bonan, 1997: Feedbacks between climate and surface water in northern Africa during the middle Holocene. *J. Geophys. Res.,* **102,** 11 087–11 101.

de Noblet, N., P. Braconnot, J. Joussaume, and V. Masson, 1996: Sensitivity of simulated Asian and African summer monsoons to orbital induced variations in insolation. *Climate Dyn.,* **12,** 589–603.

Dong, B., P. Valdes, and N. M. J. Hall, 1996: A GCM simulation of the climate 6000 years ago. *Paleoclimates,* **1,** 203–240.

Esbensen, S. K., and Y. V. Kushnir, 1981: The heat budget of the global ocean: An atlas based on estimates from marine observations. Climatic Research Institute Rep. 29, 27 pp. [Available from Climatic Research Institute and Department of Atmospheric Science, Oregon State University, Corvallis, OR 97331.]

Folland, C. K., T. N. Palmer, and D. E. Parker, 1986: Sahel rainfall and worldwide sea surface temperature. *Nature,* **320,** 602–607.

Fontaine, B., and S. Janicot, 1996: Sea surface temperature fields associated with West African rainfall anomaly types. *J. Climate,* **9,** 2935–2940.

Gadgil, S., and S. Sajani, 1998: Monsoon precipitation in the AMIP runs. *Climate Dyn.,* **14,** 659–689.

Ganopolski, A., C. Kubatzki, M. Claussen, V. Brovkin, and V. Petoukhov, 1998: The influence of vegetation–atmosphere–ocean interaction on climate during the mid-Holocene. *Nature,* **280,** 1916–1919.

Gloersen, P., and W. J. Campbell, 1991: Recent variations in Arctic and Antarctic sea-ice cover. *Nature,* **352,** 33–36.

Grenier, H., 1997: Les interactions air-mer dans le système climatique: Étude à l'aide d'un modèle couplé tri-dimensionnel océan-atmosphère-glace marine. Ph.D. disssertation, Université Catholique de Louvain, 269 pp. [Available from Lemaître Institut d'Astronomie et de Géophysique Georges Lemaître, 2 Chemin

du Cyclotron, Université Catholique de Louvain, B-1348 Louvain la Neuve, Belgium.]

Grötzner, A., R. Sausen, and M. Claussen, 1995: The impact of subgrid scale sea-ice inhomogeneities on the performances of the atmospheric general circulation model ECHAM3. *Climate Dyn.,* **12,** 477–496.

Guilyardi, E., and G. Madec, 1997: Performance of the OPA/ARPEGE-T21 global ocean–atmosphere coupled model. *Climate Dyn.,* **13,** 149–165.

——, ——, and L. Terray, 1999: The role of lateral ocean physics in the upper ocean thermal balance of a coupled ocean–atmosphere GCM. Institut Pierre Simon Laplace Sci. Note 13, 19 pp. [Available online at http://www.ipsl.jussieu.fr/modelisation/liste-notes.html]

Hall, N. M. J., and P. Valdes, 1997: An AGCM simulation of the climate 6000 years ago. *J. Climate,* **10,** 3–17.

Hellerman, S., and M. Rosenstein, 1983: Normal monthly wind stress over the World Ocean with error estimates. *J. Phys. Oceanogr.,* **13,** 1093–1104.

Hewitt, C., and J. F. B. Mitchell, 1996: GCM simulations of the climate of 6 kyr BP: Mean changes and interdecadal variability. *J. Climate,* **9,** 3505–3529.

——, and ——, 1998: A fully coupled GCM simulation of the climate of the mid-Holocene. *Geophys. Res. Lett.,* **25,** 361–364.

Hou, A. Y., 1993: The influence of tropical heating displacements on the extratropical climate. *J. Atmos. Sci.,* **50,** 3553–3570.

Janowiak, J. E., and P. A. Arkin, 1991: Rainfall variations in the Tropics during 1986–1989, as estimated from observations of cloud-top temperature. *J. Geophys. Res.,* **96,** 3359–3373.

Jolly, D., and Coauthors, 1998: Biome reconstruction from pollen and plant macrofossil data for Africa and the Arabian peninsula at 0 and 6 ka. *J. Biogeogr.,* **25,** 1007–1028.

Joussaume, S., and K. E. Taylor, 1995: Status of the Paleoclimate Modeling Intercomparison Project. *Proc. First Int. AMIP Scientific Conf.,* Monterey, CA, World Climate Research Programme, 425–430.

——, and P. Braconnot, 1997: Sensitivity of paleoclimate simulation results to season definitions. *J. Geophys. Res.,* **102,** 1943–1956.

——, and Coauthors, 1999: Monsoon changes for 6000 years ago: Results of 18 simulations from the Paleoclimate Modeling Intercomparison Project (PMIP). *Geophys. Res. Lett.,* **26,** 859–862.

Keith, D., 1995: Meridional energy transport: Uncertainty in zonal means. *Tellus,* **47A,** 30–44.

Krinner, G., C. Genthon, Z.-X. Li, and P. Le Van, 1997: Studies of the Antarctic climate with a stretched-grid general circulation model. *J. Geophys. Res.,* **102,** 13 731–13 745.

Kutzbach, J. E., and B. L. Otto-Bliesner, 1982: The sensitivity of the African–Asian monsoon climate to orbital parameter changes for 9000 years B.P. in a low-resolution general circulation model. *J. Atmos. Sci.,* **39,** 1177–1188.

——, and P. J. Guetter, 1986: The influence of changing orbital parameters and surface boundary conditions on climate simulations for the past 18 000 years. *J. Atmos. Sci.,* **43,** 1726–1759.

——, and R. G. Gallimore, 1988: Sensitivity of a coupled atmosphere/mixed layer ocean model to changes in orbital forcing at 9000 years BP. *J. Geophys. Res.,* **93,** 803–821.

——, and Z. Liu, 1997: Response of the African monsoon to orbital forcing and ocean feedbacks in the Middle Holocene. *Science,* **278,** 440–443.

——, P. J. Guetter, P. J. Behling, and R. Selin, 1993: Simulated climatic changes: Results of the COHMAP climate-model experiments. *Global Climates Since the Last Glacial Maximum,* H. E. Wright Jr. et al., Eds., University of Minnesota Press, 24–93.

——, G. Bonan, J. Foley, and S. P. Harrison, 1996: Vegetation and soil feedbacks on the response of the African monsoon to orbital forcing in the early to middle Holocene. *Nature,* **384,** 623–626.

Lamb, P. J., and R. A. Peppler, 1992: Further case studies of tropical Atlantic surface atmospheric and oceanic patterns associated with Sub-Saharan drought. *J. Climate,* **5,** 476–488.

Legate, D. S., and C. J. Willmott, 1990: Mean seasonal and spatial variability in gauge-corrected, global precipitation. *Int. J. Climatol.,* **10,** 111–127.

Levitus, S., 1982: *Climatological Atlas of the World Ocean.* National Oceanic and Atmospheric Administration, NOAA Professional Paper 13, 173 pp. and 17 microfiche.

Lindzen, R. S., and W. Pan, 1994: A note on orbital control of equator-pole heat fluxes. *Climate Dyn.,* **10,** 49–57.

Madec, G., and M. Imbard, 1996: A global ocean mesh to overcome the North Pole singularity. *Climate Dyn.,* **12,** 381–388.

Masson, V., and S. Joussaume, 1997: Energetics of the 6000-yr BP atmospheric circulation in boreal summer, from large-scale to monsoon areas: A study with two versions of the LMD AGCM. *J. Climate,* **10,** 2888–2903.

Mitchell, J. F. B., N. S. Graham, and K. J. Needham, 1988: Climate simulations for 9000 years before present: Seasonal variations and effects of the Laurentide ice sheet. *J. Geophys. Res.,* **93,** 8283–8303.

Oberhüber, J. M., 1988: An atlas based on the COADS data set: The budget of heat, buoyancy and turbulent kinetic energy at the surface of the global ocean. Max-Planck-Institut für Meteorologie Rep. 15, 42 pp. [Available from Max-Planck-Institut für Meteorologie, Bundesstr. 55, D-20146 Hamburg, Germany.]

Palmer, T. N., 1986: Influence of the Atlantic, Pacific and Indian Oceans on Sahel rainfall. *Nature,* **322,** 251–253.

Prell, W. L., and J. E. Kutzbach, 1987: Monsoon variability over the past 150,000 years. *J. Geophys. Res.,* **92,** 8411–8425.

Reynolds, R. W., 1988: A real-time global sea surface temperature analysis. *J. Climate,* **1,** 75–86.

Rind, D., 1998: Latitudinal temperature gradients and climate change. *J. Geophys. Res.,* **103** (D6), 5943–5971.

Roemmich, D., and C. Wunsch, 1985: Two trans-Atlantic sections: Meridional circulation and heat flux in the subtropical North Atlantic Ocean. *Deep-Sea Res.,* **32,** 619–664.

Royer, J. F., M. Déqué, and P. Pestiaux, 1984: A sensitivity experiment to astronomical forcing with a spectral GCM: Simulation of the annual cycle at 125 000 and 115 000 BP. *Milankovitch and Climate, Part 2,* A. L. Berger et al., Eds., Springer-Verlag, 733–763.

Ruddiman, W. F., and A. C. Mix, 1993: The North and equatorial Atlantic at 9000 and 6000 yr B.P. *Global Climates Since the Last Glacial Maximum,* H. E. Wright Jr. et al., Eds., University of Minnesota Press, 94–135.

Sadourny, R., and K. Laval, 1984: January and July performance of the LMD general circulation model. *New Perspectives in Climate Modelling,* A. Berger and C. Nicolis, Eds., Vol. 16, *Developments in Atmospheric Science,* Elsevier, 173–198.

Stein, U., and P. Alpert, 1993: Factor separation in numerical simulations. *J. Atmos. Sci.,* **50,** 2107–2115.

Terray, L., E. Sevault, E. Guilyardi, and O. Thual, 1995: The OASIS Coupler user guide version 2.0. CERFACS Tech. Rep. TR/CMGC, 123 pp. [Available from CERFACS, 42 Avenue Gaspard Coriolis, F31057 Toulouse Cedex 01, France.]

Texier, D., and Coauthors, 1997: Quantifying the role of biosphere–atmosphere feedbacks in climate change: A coupled model simulation for 6000 yr BP and comparison with paleodata for northern Eurasia and northern Africa. *Climate Dyn.,* **13,** 865–882.

Trenberth, K., and A. Salomon, 1994: The global heat balance: Heat transports in the atmosphere and ocean. *Climate Dyn.,* **10,** 107–134.

Wang, T., Y. Lin, H. F. M. Semazzi, and G. S. Janowitz, 1996: Response of a stably stratified atmosphere to large-scale diabatic forcing with applications to wind patterns in Brazil and the Sahel. *J. Geophys. Res.,* **101** (D3), 7049–7073.

Wright, H. E., Jr., J. E. Kutzbach, T. Webb III, W. F. Ruddiman, F. A. Street-Perrott, and P. J. Bartlein, Eds., 1993: *Global Climates Since the Last Glacial Maximum.* 1st ed. University of Minnesota Press, 169 pp.

Yu, G., and S. P. Harrison, 1996: An evaluation of the simulated water balance of northern Eurasia at 6000 yr BP using lake status data. *Climate Dyn.,* **12,** 723–735.